The peculiarities of convective motions in the fluid with the quadratic density-temperature dependence

Daria V. Kuznetsova Ilias N. Sibgatullin
morven9@yandex.ru

Abstract

A horizontal layer of fluid with the quadratic density-temperature dependence is studied. A typical example for such a fluid is fresh water at the atmospheric pressure near the point of the density maximum which is at the temperature 3.98°C. The horizontal boundaries are isothermal and stress-free. The position of the maximum of density is determined by the temperatures at the boundaries. The layer in the static state can be separated into two parts: the sublayer which can be unstable under the certain circumstances and the sublayer which is stable. The arising convective motions lead to the interaction of these sublayers and to the development of the motions in the whole layer.

The height of the layer is fixed while the temperature difference at the boundaries is varied. Two-dimensional problem is studied in a periodicity cell with the absence of the horizontal flow through the vertical boundaries, the length of the periodicity cell chosen according to the additional simulations at large horizontal scales. The pseudospectral method was used with spectral resolution up to 1024x256. The point of the density maximum is supposed to be located in the middle plane of the layer in conductive state.

The evolution of the flow with the increase of the supercriticality is studied. Branches of hysteresis are found with the coexistence of different solutions. The sequence of bifurcations leading to chaos is described, with the subcritical Neimark–Sacker bifurcation with the phase locking resulting in periodic-2 regime on a torus after periodic regime.

1 Introduction

When stable and unstable layers of any fluid are connected, the disturbances arise in the unstable part. They penetrate from the unstable sublayer to the stable one, so this phenomenon is called penetrative convection. The most widespread example of penetrative convection on the Earth is convection in fresh water at the atmospheric pressure and temperatures close to the point of the density maximum. It is known that fresh water has a density maximum which can be approximately taken as 4°C at the atmospheric pressure. The density–temperature dependence for temperatures from 0° to 10°C can be approximated then by the quadratic function with the maximum at 4°C. Stable and unstable sublayers are formed due to the presence of the density maximum.

Convection in the water layer with the quadratic density–temperature dependence was mathematically formulated in [1] for the first time. Linearized and weakly nonlinear formulations of the problem were investigated and the possibility of subcritical bifurcation for transition from conductive state to steady motions was predicted. Then, steady and

periodic regimes were investigated for the same or similar problem formulation (e.g. [2]-[7]). Some experiments were also done, e.g. [8, 9] where steady regimes were obtained and two-dimensional rolls and different three-dimensional configurations were shown.

Horizontal scales for steady and periodic solutions, hysteresis domains and quasiperiodic regimes are also described in [11, 12] where some results concerning the evolution of two-dimensional solution with equal heights of stable and unstable layers are presented.

2 The formulation of the problem

The horizontal layer of water of the height h is confined between $z = 0$ and $z = h$. The boundaries are stress-free, impermeable, and isothermal with the temperatures T_b at the lower boundary and T_u at the upper boundary. It is supposed that $\min(T_\mathrm{b}, T_\mathrm{u}) < T_4 < \max(T_\mathrm{b}, T_\mathrm{u})$, then the point of density maximum $T_4 = 4°\mathrm{C}$ will be located inside the layer.

The equation of state is taken as in [1]

$$\rho = \rho_4 \left(1 - \alpha_4 (T - T_4)^2\right), \tag{1}$$

where ρ_4 is the density at 4°C, $T_4 = 4°\mathrm{C}$, $\alpha_4 = 7.68 \cdot 10^{-6}\,(°\mathrm{C})^{-2}$.

The variables describing the motion are represented as the sum of functions in conductive state and the perturbations from this state: $f = f_\mathrm{m} + f_0(z) + f'$, where f_m is some constant reference value, $f_\mathrm{m} + f_0(z)$ is the distribution in conductive state and f' is the deviation from conductive state.

The Boussinesq approximation is taken for the system of equations that consists of the Navier–Stokes equation, continuity, and energy equations ([10], [13]). The functions and variables will be nondimensionalized as follows: $T = (T_\mathrm{b} - T_\mathrm{u})\,T^*$, $\rho = \rho_4 \rho^*$, $\mathbf{v} = (\kappa/h)\,\mathbf{v}^*$, $t = (h^2/\kappa)\,t^*$, $p = (\rho_4 \kappa \nu / h^2)\,p^*$, $(x, y, z) = h(x^*, y^*, z^*)$ where asterisks denote the non-dimensional variables.

As the functions in conductive state satisfy the system of equations in the Boussinesq approximation, the non-dimensional equations for the disturbances can be written in the following way (asterisks are dropped):

$$\frac{\partial \mathbf{v}}{\partial t} + (\mathbf{v} \cdot \nabla)\mathbf{v} = -\sigma \nabla p + \sigma \triangle \mathbf{v} + \sigma \frac{R}{\lambda^5} (T + 2\lambda - 2z)\,\mathbf{e}_\mathrm{z}$$

$$\frac{\partial T}{\partial t} + (\mathbf{v} \cdot \nabla)\,T - w = \triangle T$$

$$\mathrm{div}\mathbf{v} = 0$$

where non-dimensional parameters are:

$$\sigma = \frac{\nu}{\kappa}, \quad R = \frac{g\alpha_4}{\nu\kappa} \frac{h^3}{\lambda^3} (T_b - T_4)^2, \quad \lambda = \frac{T_\mathrm{b} - T_4}{T_\mathrm{b} - T_\mathrm{u}}.$$

Here σ is the Prandtl number, R is the Rayleigh number, λ specifies position of point of density maximum inside the layer. The dimensional parameters are: ν — the kinematic viscosity, κ — the coefficient of the thermal diffusivity, g — the gravitational acceleration.

The viscosity and thermal diffusivity are supposed to be constant and the values used here are the corresponding values for water at 4°C. Then the Prandtl number is constant and equal to $\sigma = 11.5968$. The height of the layer is equal to 0.1 m and the temperature difference at the boundaries is varied. We suppose that the point of the density maximum is located at $z = 1/2h$.

Two-dimensional problem is examined. The periodicity cell with stress-free vertical boundaries is considered. (The horizontal scale of the cell was chosen with particular attention and it will be discussed further.)

The velocity components $\mathbf{v} = \{u, w\}$ and temperature T are expressed by the Galerkin method as truncated Fourier series with time-dependent coefficients. Taking into account the boundary conditions, the expansion is the following:

$$u = \sum_{m=0}^{M/2} \sum_{n=0}^{N/2} U_{mn}(t) \sin(\pi m \alpha x) \cos(\pi n z), \; w = \sum_{m=0}^{M/2} \sum_{n=0}^{N/2} W_{mn}(t) \cos(\pi m \alpha x) \sin(\pi n z),$$

$$T = \sum_{m=0}^{M/2} \sum_{n=0}^{N/2} \tau_{mn}(t) \cos(\pi m \alpha x) \sin(\pi n z).$$

The introduced horizontal wave number α characterizes the horizontal scale of the periodicity cell which is equal to $2L = 2/\alpha$.

It must be noted that the expressions for the functions involve the additional symmetry: if the periodicity cell is $[-L, L] \times [0, 1]$, then the solution is symmetric with respect to $x = 0$ and is really calculated in $[0, L] \times [0, 1]$. Then the results will be further represented only for the computational domain.

The expansion into the Fourier series allows to obtain the system of ordinary differential equations, then an initial-value problem is posed. The Bulirsch–Stoer method [14] was used to solve the equations. The nonlinear terms were computed by means of the pseudospectral method [15]. Libraries for Fast Fourier Transform (http://fftw.org) were used. The number of Fourier harmonics was up to 1024x256.

3 Hysteresis

Now we will consider evolution of solutions with the increase of Rayleigh number in the computational domain with horizontal length $2L_0$, where $L_0 = \sqrt{2}$ — the value taken from the linearized theory of the classical Rayleigh–Bénard convection.

Several different kinds of solutions were found for the chosen horizontal length of the computational domain.

The features of solutions can be illustrated by the dependence of the Nusselt number on the temperature difference at the boundaries $\mathrm{Nu_T}(\Delta T)$, where $\triangle T = T_\mathrm{b} - T_\mathrm{u}$ and $\mathrm{Nu_T} = \langle \partial T/\partial z \rangle_{z=0}$. (Here the angular brackets denote x–averaging over the horizontal length of the periodicity cell.) This dependence is plotted in Fig. 1. The branches of solutions are denoted in Fig. 1 by I, II, III, IV.

In Fig. 2a,b the same dependence $\mathrm{Nu_T}(\Delta T)$ is shown for the domain corresponding to the small supercriticalities. One can see (Fig. 2a) that near the transition from static to steady (non-zero velocity) regime the branches I, II and IV coexist while the branch III is absent. Then with the increase of the supercriticality the branch IV becomes unstable, and the branch III appears (Fig. 2b).

In Fig. 3 and 4 streamlines for steady regimes on the all branches are shown. One can see that the solutions on the branches I, II and III have similar structure which consists of several vortices occupying the large part of the layer and some smaller vortices located near the upper boundary. The number of large vortices is 3 (Fig. 3a), 4 (Fig. 3b) and 8 (Fig. 4a) for the solutions on the branches I, II and III, correspondingly, and the number of small vortices is equal to the number of large ones.

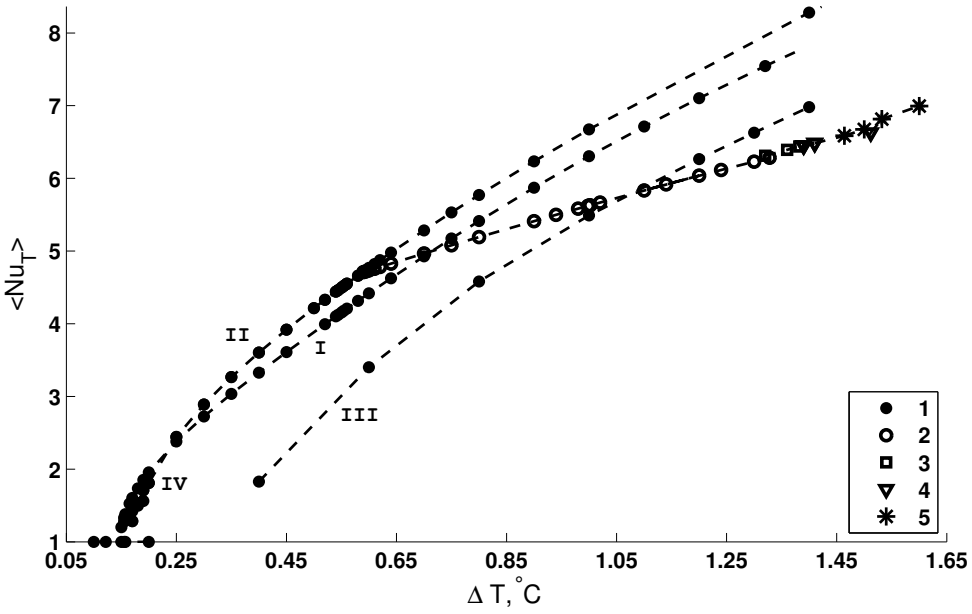

Figure 1: The dependence of the time-averaged Nusselt number on the supercriticality (the temperature difference at the boundaries). 1, steady or conductive regime; 2, periodic regime; 3, periodic-2 regime; 4, quasiperiodic regime; 5, stochastic regime. The numbers I, II, III, IV denote the branches of hysteresis.

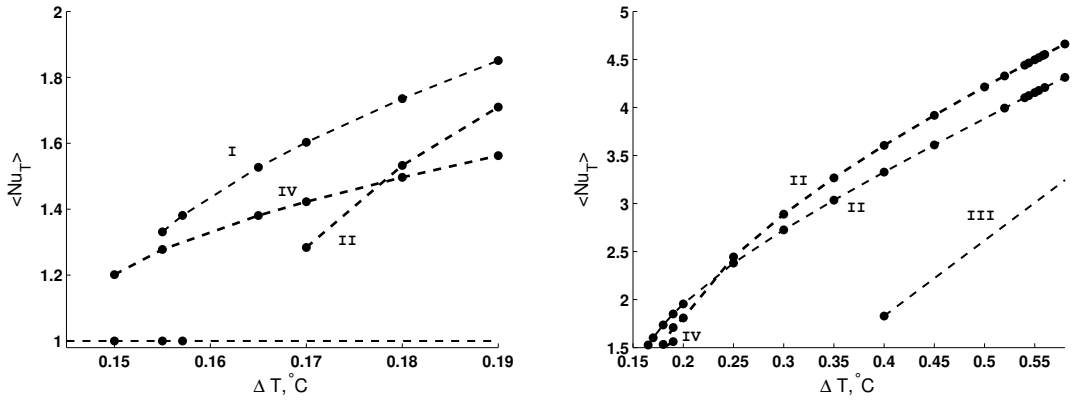

a b

Figure 2: The dependence of the time-averaged Nusselt number on the supercriticality (the temperature difference at the boundaries) for the values corresponding to small supercriticalities. The numbers I, II, IV denote the branches of hysteresis.

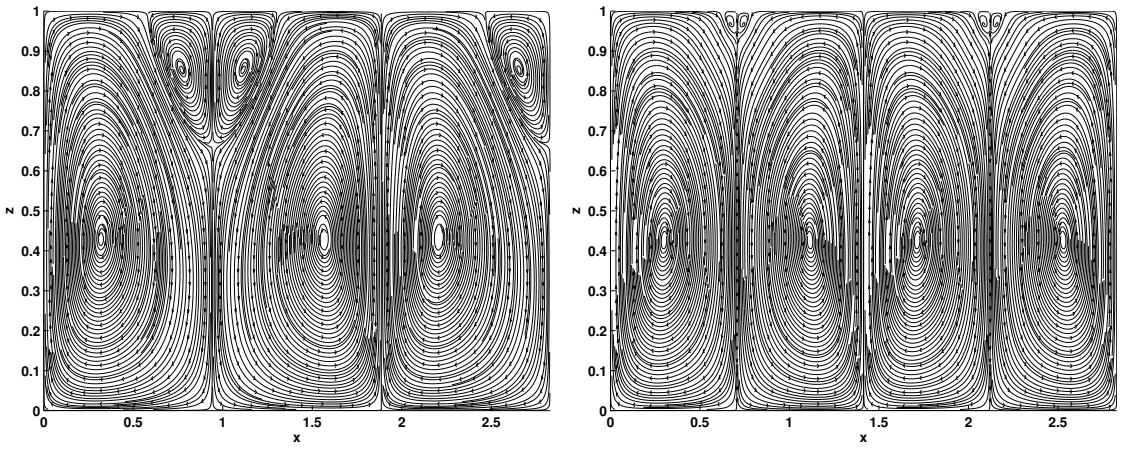

a b

Figure 3: Streamlines for the steady solutions on the branches I and II.

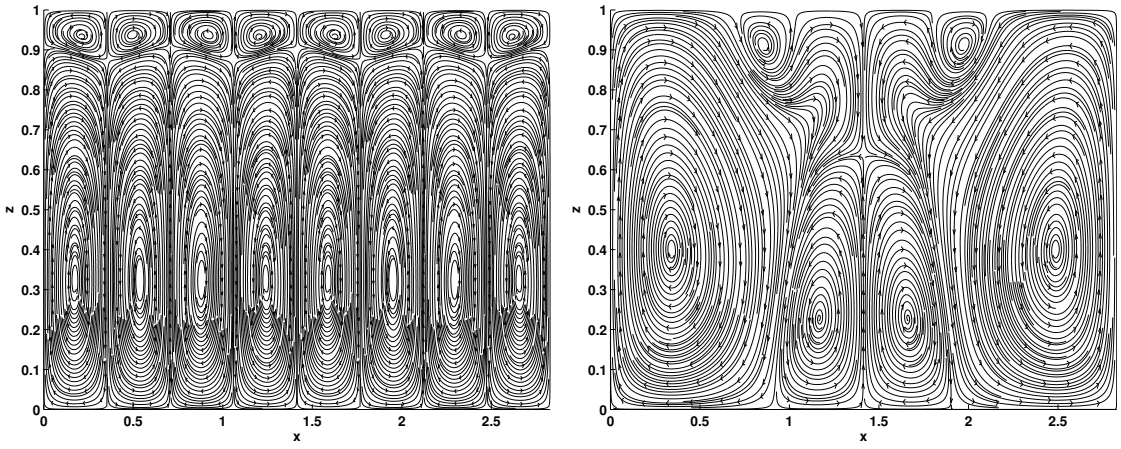

c d

Figure 4: Streamlines for the steady solutions on the branches III and IV.

The branch IV has a completely different structure of the solution (Fig. 4b). There are two large vortices, two smaller vortices near the lower boundary, and two small vortices near the upper boundary.

The branches I and IV have only steady solutions while the branches II and III have also periodic solutions (these solutions for the branch IV are not shown here). On the branch II, there is a transition to chaos for larger values of the supercriticality.

4 Transition to chaos on the branch II

After the steady solutions, there appear a periodic solution on the branch II through the Poincaré–Andronov–Hopf bifurcation. After this point the branch II divides into two parts corresponding to periodic and steady regimes. Steady solution is unstable and can be obtained by taking a previous steady solution as the initial condition to compute a new one with a higher Rayleigh number. It is also stable to arbitrary perturbations of non-zero harmonics, but will be unstable to perturbations that are product of the periodic solution

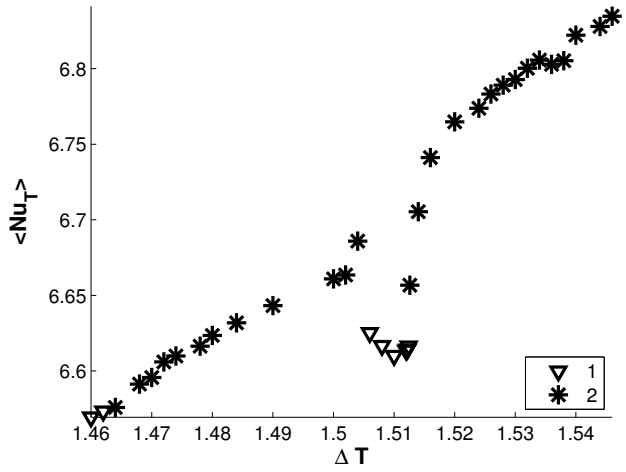

Figure 5: Transitional regimes: the dependence of the Nusselt number on ΔT. 1, quasiperiodic regimes; 2, intermittent regime

for the same Rayleigh number and an arbitrary small number. (It must be noted that by choosing the special initial conditions this steady unstable solution can be obtained even for very large values of the supercriticality.)

With the increase of the supercriticality, the periodic motion becomes unstable and the Neimark–Sacker bifurcation occurs with the phase locking [12]. This means that after periodic regime, periodic-2 regime on a torus appears instead of the quasiperiodic regime. Both periodic and periodic-2 motions exist until the certain value of the supercriticality when periodic regime becomes unstable.

Then, there is a transition from periodic-2 to quasiperiodic motion which will be labeled as Q^1. With the increase of the supercriticality, after the quasiperiodic mode Q^1 strong bursts appear on the background of the base quasiperiodic motion. This intermittent regime soon disappears and new quasiperiodic motion Q^2 arises (different from Q^1).

With the further increase of supercriticality new intermittent regime appears but now the turbulent bursts present on the background of the regime Q^2.

In Fig. 5 the dependence of the Nusselt number on the temperature difference at the boundaries is shown for quasiperiodic and intermittent regimes. It can be seen that the mean value of the Nusselt number drops as compared with its previous values after Q^2 mode appears.

5 Conclusions

The distinctive features of penetrative convection with the density maximum in a water layer were investigated in a chosen length of the periodicity cell. The four main branches of hysteresis are found. The transition to chaos through quasiperiodic and intermittent regimes which occurs at one of the branches of hysteresis was described. When the steady regime becomes unstable, the periodic motion appears which then transforms into periodic-2 on a torus after the subcritical Neimark–Sacker bifurcation with the phase locking (so the quasiperiodic regime does not manifest itself immediately after the periodic regime). Then, quasiperiodic motion sets in. With the increase of the supercriticality, strong bursts are noticeable on the background of the initial regime i.e. we obtain intermittency on

the background of quasiperiodic motion. The window of quasiperiodicity exists inside the range of intermittent solutions. Then, intermittency arises on the background of the new quasiperiodic regime.

Acknowledgements

This study was supported by the Russian Foundation for Basic Research, project no. 12-01-31460 mol_a. Computations were done at the supercomputer systems "Chebyshev" and "Lomonosov" of Lomonosov Moscow State University.

References

[1] Veronis G. 1963, Astrophys. J. V.137, pp. 641–663.

[2] Musman S. 1968, J. Fluid Mech., V.31, pp. 343–360.

[3] Blokhin A. S., Blokhina N. S., Makaeva O. S. 1973, Dokl. Akad. Nauk SSSR, V.201, pp. 75–78.

[4] Moore D. R., Weiss N. O. 1973, J. Fluid Mech., V.61, pp. 553–581.

[5] Blake K. R., Poulikakos D., Bejan A. 1984, Phys. Fluids, V.27, pp. 2608–2616.

[6] Tong W., Koster N. J. 1993, Wärme- und Stofftübertragung, V.29, pp. 37–49.

[7] Nadolin K. A. 1989, Fluid Dynamics, V.24, pp. 35–41.

[8] Tankin R., Farhadieh R. 1971, Int. J. Heat Mass Transfer, V.14, pp. 953–960.

[9] Large E. D. 2010, An experimental investigation of penetrative convection in water near 4C, PhD thesis The Ohio State University.

[10] Nadolin K. A. 1996, Fluid Dynamics, V.31, pp. 193–205.

[11] Kuznetsova D. V., Sibgatullin I. N. 2011, Doklady Physics, V.56, pp. 271–274.

[12] Kuznetsova D. V., Sibgatullin I. N. 2012, Fluid Dynamics Research. V.44, p. 031410.

[13] Spiegel E. A., Veronis G. 1960, Astrophys. J., V.131, pp. 442–447.

[14] Press W. H., Teukolsky S. A., Vetterling W. T., Flannery B. P. 2007, Numerical Recipes 3rd Edition, Cambridge University Press.

[15] Fletcher C. A. J. 1984, Computational Galerkin methods, New York: Springer–Verlag.

Daria V. Kuznetsova, Institute of Mechanics of Lomonosov Moscow State University, Michurinsky, 1, Moscow, Russia
Ilias N. Sibgatullin, Institute of Mechanics of Lomonosov Moscow State University, Michurinsky, 1, Moscow, Russia